ADVANCED MATERIALS
www.advmat.de

An Artificial Flexible Visual Memory System Based on an UV-Motivated Memristor

Shuai Chen, Zheng Lou, Di Chen, and Guozhen Shen**

For the mimicry of human visual memory, a prominent challenge is how to detect and store the image information by electronic devices, which demands a multifunctional integration to sense light like eyes and to memorize image information like the brain by transforming optical signals to electrical signals that can be recognized by electronic devices. Although current image sensors can perceive simple images in real time, the image information fades away when the external image stimuli are removed. The deficiency between the state-of-the-art image sensors and visual memory system inspires the logical integration of image sensors and memory devices to realize the sensing and memory process toward light information for the bionic design of human visual memory. Hence, a facile architecture is designed to construct artificial flexible visual memory system by employing an UV-motivated memristor. The visual memory arrays can realize the detection and memory process of UV light distribution with a patterned image for a long-term retention and the stored image information can be reset by a negative voltage sweep and reprogrammed to the same or an other image distribution, which proves the effective reusability. These results provide new opportunities for the mimicry of human visual memory and enable the flexible visual memory device to be applied in future wearable electronics, electronic eyes, multifunctional robotics, and auxiliary equipment for visual handicapped.

Eyes, acting as perceptual organs to sense light, provide crucial visual information to distinguish the size, shape, color, and brightness of objects, distance, and location sensation, smoothness, and roughness of object's surface, etc.[1,2] Human visual memory is formed by receiving image information from retina and allows individual to remember the impressions of images our eyes observed, as illustrated in **Figure 1**a.[3–6] The recent researches for mimicking human visual system have achieved momentous progress by utilizing image sensor arrays mostly to realize the recognition function for perceived images.[7–12] Unfortunately, even though the current image sensor devices can identify some designated images in real time,[9–11] there are few studies having the capacity to retain and memorize the detected image information even after removing the external image stimulation compared with human visual memory. The deficiency between the image sensor arrays and visual system inspired the logical integration of image sensors and memory devices to realize the sensing and memory process toward light information for the bionics design of human visual memory.

Resistive switching memory device provides a promising physical infrastructure for imitating memory function of human nervous system. It is a memristor with metal–insulator–metal sandwich configuration as the two-terminal geometry of synapses essentially, the resistance of which can be switched electrically between high resistance state (HRS) and low resistance state (LRS), corresponding to the two logic states: OFF (0) state and ON (1) state, respectively.[13–17] With resistive switching memory devices, researchers have realized the ability, such as synaptic plasticity, neuromorphic computing, and it is feasible for memory device to mimic biological synapses due to the homophyly between the working mechanism of memory device and the transinformation behaviors of synapses among neurons.[18–21] Inspired by these features, the electronic integration of image sensors and memory devices will provide an opportunity to realize the mimic of human visual memory. As we know, oxide electronic materials such as In_2O_3 are excellent UV light-sensitive materials and Al_2O_3 are good bipolar resistive switching materials, which have been exploited for a wide range of applications including optoelectronics, thermoelectrics, and piezoelectrics, etc.[22,23] In this work, we design a bioinspired flexible visual memory system by the rational integration of UV image sensors and resistive switching memristors based on oxide electronic materials (Figure 1b and Figure S1, Supporting Information). The resistance switching

Dr. S. Chen, Prof. D. Chen
College of Physics and Mathematics and Beijing Key Laboratory for Magneto-Photoelectrical Composite and Interface Science
University of Science and Technology Beijing
Beijing 100083, China
E-mail: chendi@ustb.edu.cn
Dr. S. Chen, Dr. Z. Lou, Prof. G. Z. Shen
State Key Laboratory for Superlattices and Microstructures
Institute of Semiconductors
Chinese Academy of Sciences
Beijing 100083, China
E-mail: gzshen@semi.ac.cn
Prof. G. Z. Shen
College of Materials Science and Opto-Electronic Technology
University of Chinese Academy of Sciences
Beijing 100049, China
The ORCID identification number(s) for the author(s) of this article can be found under https://doi.org/10.1002/adma.201705400.

DOI: 10.1002/adma.201705400

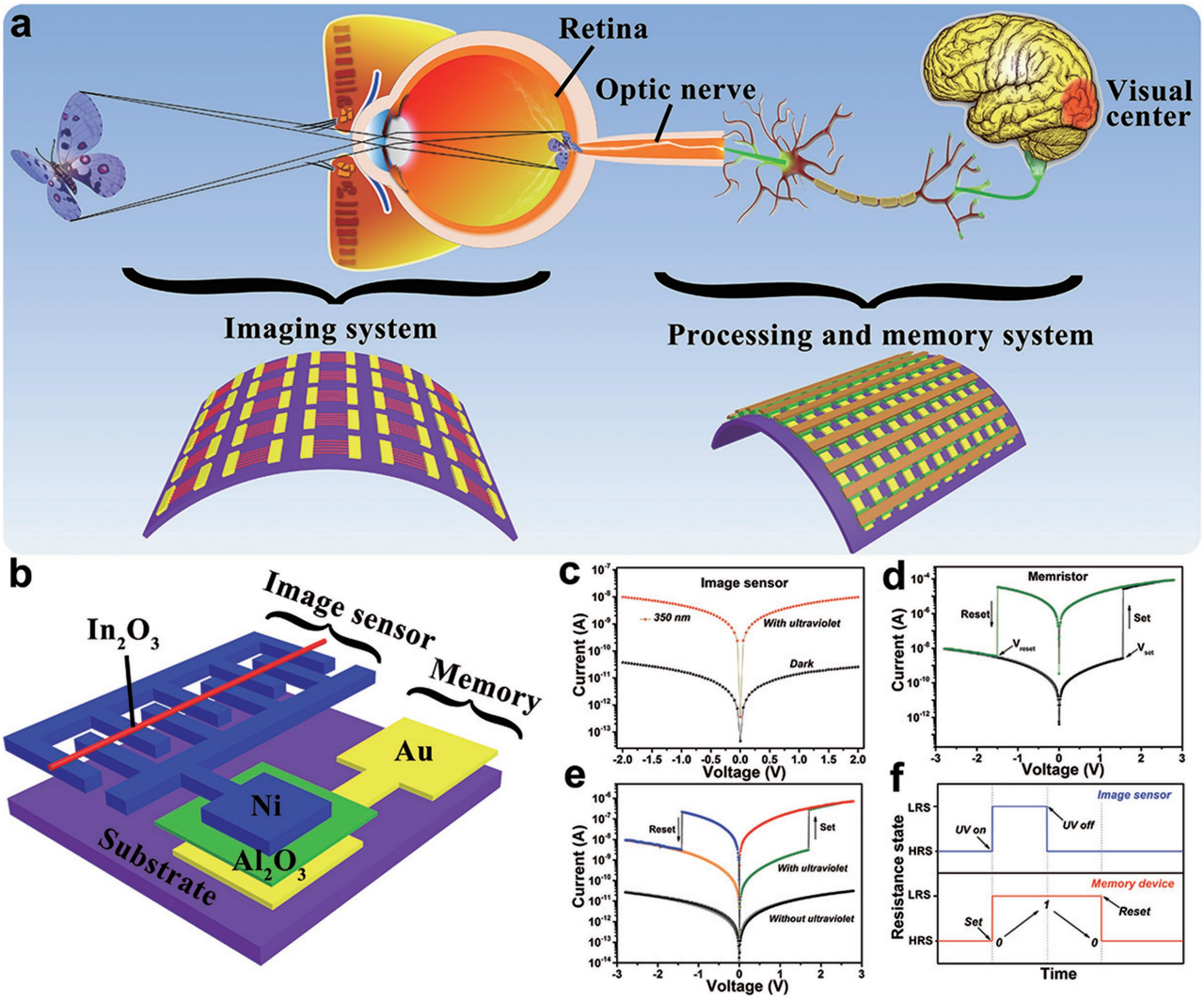

Figure 1. Visual memory devices based on resistive switching memory devices and resistive image sensors to imitate human visual memory. a) Schematic diagrams of human visual system when a butterfly was observed by eyes. b) Schematic illustration of the bioinspired visual memory unit integrated by image sensor and resistive switching memory device. c) Typical *I*–*V* curves of the image sensor under dark and 350 nm UV light. d) Typical *I*–*V* curves of the memristor. e) Typical *I*–*V* characteristic of the bioinspired visual memory unit with and without UV light illumination. f) Schematic illustration of the function of resistance states between image sensor and memory device.

of image sensors by sensing applied light can be recorded in the nonvolatile memory devices, thus realizing the detection and memory capacities toward light as human visual memory.

Figure 1b shows the schematic illustration of our bioinspired visual memory unit, where the top electrode of the memory device unit is replaced by one electrode of the two-terminal image sensor, constituting an integrated visual memory device in series. The configuration of interdigital electrodes can adjust the dark current of the image sensor to match with the resistance states of the memristor by regulating the numbers of multipled semiconductor micrometer-sized wires (SMWs). Resistance state of the image sensor can be motivated by external UV light from HRS to LRS as shown in Figure 1c and the resistance switching of memristor can be controlled by the set and reset voltages as shown in Figure 1d. The reduction of resistance in image sensor will lead to the increase of partial voltage on the tandem memristor unit, resulting in the resistance switching of memristor from OFF state to ON state and the light information will be stored in memory device (Figure 1e,f). After removing the applied light, the information can be retained in the memory device until a reset voltage applied.

A home-built direct-printing system to fabricate aligned SMWs arrays is illustrated in **Figure 2**a. Taking advantage of two-dimension (*X*–*Y* axis) moving platform and near-field electrospinning technology, this system can print various aligned organic/inorganic micrometer-sized wires on rigid or flexible substrates. The detailed printing process for In_2O_3 SMWs has been explained in the Experimental Section. Different from conventional electrospinning, near-field electrospinning utilizes small DC voltage (lower than 2 kV), short electrospinning distance (0.5–1.4 mm), and ultrafine stainless steel nozzle with

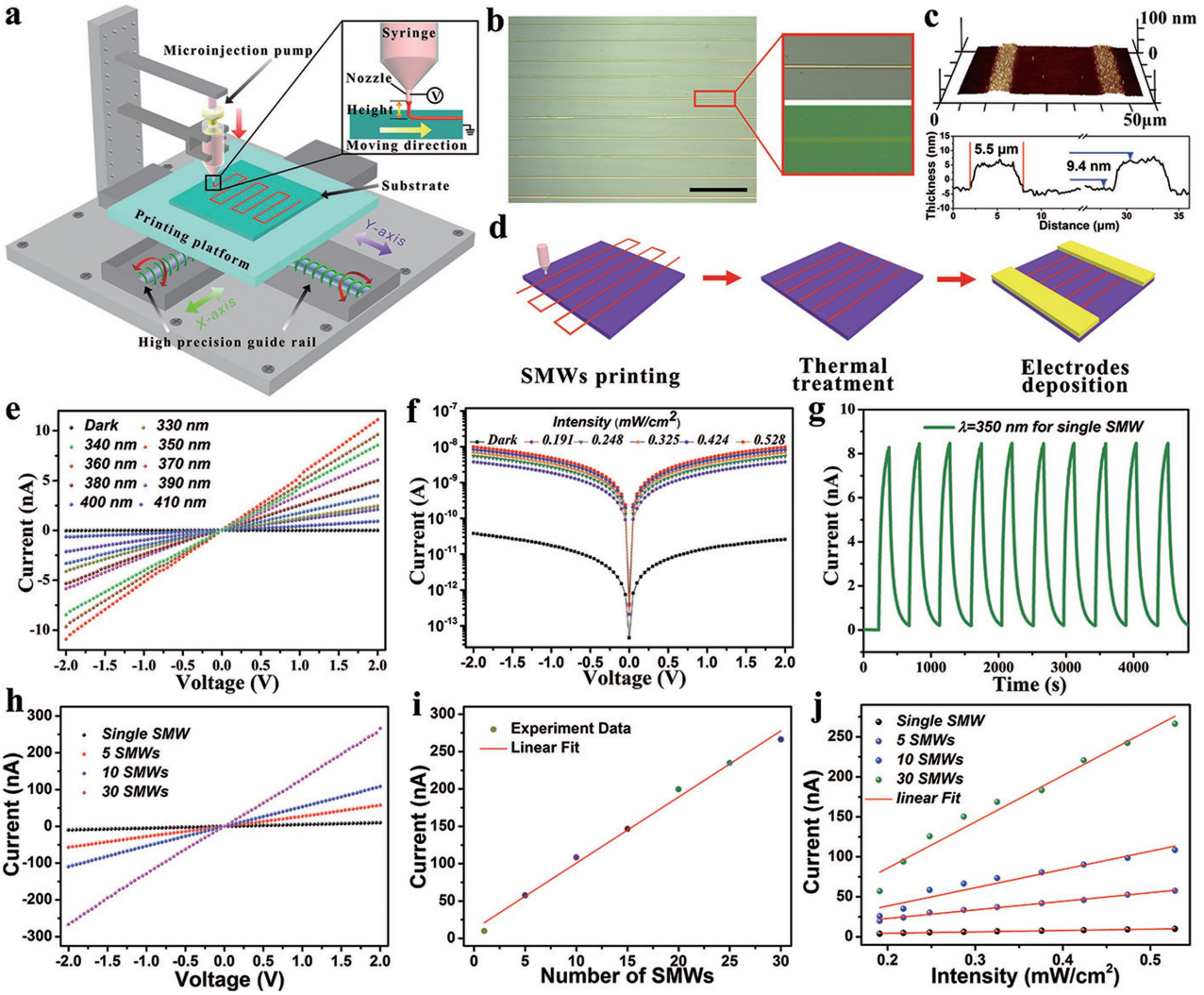

Figure 2. Direct printing of aligned SMWs and photoresponse performance. a) Schematic diagram of near-field direct-printing system. b) Optical images of the as-printed In_2O_3 SMWs with an adjacent spacing of 20 μm. The magnifying images are the single In_2O_3 SMW before and after calcination. Scale bar, 50 μm. c) AFM image of two aligned SWMs after calcination and cross-sectional analysis. d) Schematic illustration of the process to fabricate aligned In_2O_3 SMWs image sensor. e) Typical *I*–*V* curves of printed single In_2O_3 SWM image sensor measured under dark and various UV wavelengths. The light intensity was kept constant at 0.528 mW cm^{-2}. f) Typical *I*–*V* curves of single In_2O_3 SWM image sensor under dark and 350 nm light illumination with different light intensities. g) Time domain photoresponse of the image sensor based on printed single In_2O_3 SMW under 350 nm UV illumination at +1 V bias voltage. h) Typical *I*–*V* curves of the image sensor based on different numbers of printed In_2O_3 SWMs at 350 nm light illumination. i) The dependence of photocurrents on numbers of printed In_2O_3 SMWs. j) The dependence of photocurrents on light intensity under different numbers of printed In_2O_3 SMWs at +1 V bias voltage.

an inner diameter of about 130 μm. Under the effect of applied electrical field, Taylor cone can be formed at the tip of nozzle because the electrostatic force stretches the viscous precursor solution and while it reaches to the critical electrical field, electrostatic forces can overcome the surface tension forces of solution, thus a jet can be induced from the tip of Taylor cone.[24,25] Typically, the critical electrical field of near-field electrospinning is employed on the order of 10^6 V m^{-1} which is larger than that of conventional electrospinning (10^5 V m^{-1}) for that the surface tension of polymer droplet increases as nozzle diameter decreases. However, the short electrospinning gap leads to a reduced influence of Coulombic repulsion force in the polymer jet and an effective suppression of instable whipping and perturbation behaviors of jetted solution.[26–28] Meanwhile, there is a deficient space between the Taylor cone tip and substrate to further stretch the precursor fibers and the solvent in the polymer jet does not have enough time to fully evaporate, which result in a large diameter of as-spun fiber compared to that of conventional electrospinning.

The aligned SMWs can be prepared with the movements of the platform along *X*–*Y* axis by inputting a programmed moving trajectory into computer control system to control the moving speed and trajectory of *X*–*Y* axis. Particularly, the morphology of the straight SWMs and interval between the adjacent SWMs can be tuned by controlling the moving speed of *X* and *Y* axes, respectively (Figure S2, Supporting Information).

Through setting the interval of y axis between the adjacent two lines, the printing density of SMWs can be controlled as expectation (>5 μm). Figure 2b shows the as-printed aligned In_2O_3 SMWs arrays with a regular interval set as 20 μm before calcination. The magnifying images are morphologies of single In_2O_3 SMW before and after calcination at 400 °C. The atomic force microscope (AFM) image (Figure 2c) and histogram in Figure S4 (Supporting Information) reveal the printed two SMWs had parallel orientation and the SMWs owned a thickness of 9.4 nm and a uniform width of 5.5 μm. In this fashion, SMWs arrays with different patterns are fabricated on either rigid or flexible substrates by adjusting printing parameters (Figure S3, Supporting Information). The unique superiority to prepare aligned SMWs arrays provides useful paths for future multifunctional integration in the fields of functional devices and circuits.

For the UV image sensor, In_2O_3 SMWs are employed as the photosensitive materials due to its wideband, high photosensitivity, and effective charge transport. In order to investigate the optoelectronic properties, the printed In_2O_3 SWMs arrays are calcined rapidly to remove the organic component and induce the crystallization after printing SWMs of precursor solution. Then, Au electrodes are deposited by thermal evaporation on both sides of the SWMs arrays with a spacing of ≈40 μm between two adjacent electrodes (Figure 2d).

For the image sensor based on single In_2O_3 SMW on SiO_2/Si substrate, a monochromatic light is illuminated vertically on the device and the corresponding photoresponse properties are determined. As shown in Figure 2e, a peak response wavelength of 350 nm can be obtained from the current–voltage (I–V) characteristic curves of image sensor when exposed to various UV wavelengths and under dark conditions. Moreover, the device has a broad response range of wavelengths from 330 to 410 nm. Figure 2f illustrates the I–V characteristics of the image sensor in the dark and under different light intensities of 350 nm UV illumination, respectively. It can be observed that the photocurrent increases as the light intensity increases which can be attributed to the photogenerated charge carrier efficiency is proportional to the absorbed photon flux. Under a constant light intensity of 0.528 mW cm^{-2}, the absolute current increased from dark current to ≈10 nA at a bias voltage of 1 V with a calculated on/off ratio (I_{light}/I_{dark}) up to four orders of magnitude, which is several orders of magnitude higher than the previously reported In_2O_3-based nanostructure image sensors.[29–32] The transport mechanism of In_2O_3 SWMs-based image sensor has been explained in the Supporting information.[33] The high on/off ratio is owing to the high photocurrent and low dark current for the enhanced crystallinity of In_2O_3 by near-field electrospinning process. The applied electric field during printing process leads to an increasing ionic concentration of precursor solution which accumulates around Taylor cone. The high concentration of mobile ions in precursor can result in an enhanced crystallinity and existence of grain boundaries of In_2O_3 after thermal calcination, thus greatly suppressed the dark current of image sensor.[24,26]

Noticeably, the photoresponse behaviors of the image sensors can be dominated by adjusting the numbers of printed SMWs. As essential prerequisite, the reproducibility and uniformity of the single SMW-based image sensor are demonstrated, indicating no obvious decay of dynamic photoresponse from HRS to LRS while turn on and off UV light periodically (Figure 2g). The dark current and photocurrent for 50 image sensors are distributed in the confined regions with little fluctuation, revealing a uniformity and stability of photoresponse for image sensor fabricated by near-field direct-printing technology (Figure S6, Supporting Information). Thus, the level of photocurrent can be improved by printing aligned SMWs with more numbers. Since the number of aligned SWMs can be easily controlled by the direct-printing system, the devices with 1, 5, 10, 15, 20, 25, and 30 SMWs are fabricated in order to investigate the relationship between photocurrent and numbers of SMWs. For the image sensors based on different numbers of In_2O_3 SMWs (Figure 2h,i), the dependence of photocurrents on SMWs numbers is shown under same light intensity and the results prove that the photocurrent level increased linearly with the numbers of printed SMWs. From Figure 2j, it can be obtained that the photocurrent increased rapidly with further increase of the light intensity for all the printable image sensors. The results can be fitted to a power law, $I = AP^{\theta}$, where I is the photocurrent, A is a constant, P is the light intensity, and θ is an empirical value which determines the response of photocurrent to light intensity.[8,10] As shown for all the image sensors, there is a strong dependence between the light intensity and photocurrent, and the fitting relationship of the experimental data exhibits an exponential function of $I \sim P^{1.01–1.04}$, suggesting an excellent photoresponse capability of the printed In_2O_3 SMWs. The dependencies can be explained by the undersaturated situation of the photoresponse at the low light intensities and the photogenerated charge carrier efficiency is proportional to the absorbed photon flux. The superior relationships indicate that the characteristics of the image sensor can be controlled by adjusting the numbers of printed SWMs, providing an effective guarantee for the integration of visual memory device.

The visual memory device is integrated by resistive switching memristor and image sensor based on printed In_2O_3 SMWs and one integrated visual memory unit corresponds to one pixel unit of image. The memristor can be triggered to achieve LRS by applied positive voltage (V_{set}) and only a negative voltage (V_{reset}) can erase it from LRS to HRS in a resistance switching cycle, which is equivalent to the read-in (ON state) and erased (OFF state) process in digital memory cell. Herein, we take 23 nm Al_2O_3 layer as the memory layer to establish Ni/Al_2O_3/Au architecture (**Figure 3**a,b), providing excellent resistance switching behaviors, such as long-term retention, high endurance, and stable switching performance as same as nonvolatile memory device. The switching characteristics of Ni/Al_2O_3/Au memristor are illustrated in Figures S8–S11 (Supporting Information). To integrate visual memory device with a fast write speed and accurate information storage, the resistance of the image sensor should be matched with that of the memristor by adjusting the numbers of printed In_2O_3 SMWs as explained in Figure S12 (Supporting Information). The switching characteristics of the visual memory device were performed by applying a periodic voltage (–2.8 V → 2.8 V → –2.8 V) under a direct current sweeping mode (Figure 1e). Only in the existence of UV light, light information can be memorized and erased from the memory device by voltage sweep. Notably, just like the

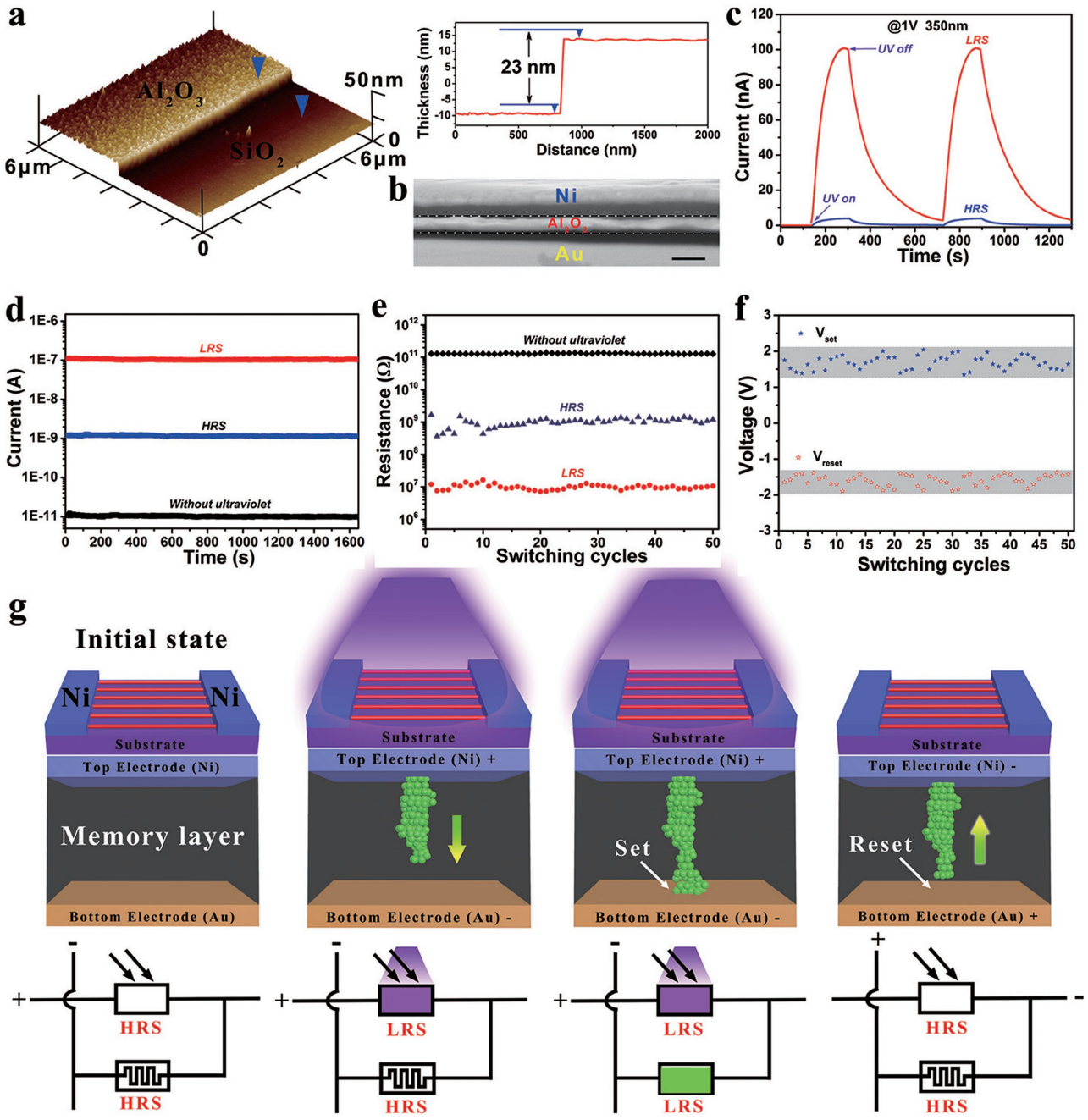

Figure 3. Switching characteristics of the visual memory unit under UV light illumination. a) AFM image and cross-sectional analysis of selected region in Al_2O_3 memory layer. b) A layer-by-layer structure for cross-sectional SEM image of memristor unit. Scale bar, 50 μm. c) Time domain photoresponse of the visual memory unit at HRS and LRS responding to 350 nm UV light at +1 V bias voltage. d) Retention characteristic of the visual memory unit at +1 V bias voltage. e) Endurance test of the visual memory unit for 50 switching cycles. f) Distribution of the set voltage and reset voltage for 50 switching cycles. g) Schematic illustrations of switching mechanism analysis.

light information storage and information reading, the resistance states after set/reset process can be recorded in memristor and read momentarily by checking the on/off state of memristor even if removing the applied UV light. In Figure 3c, the visual memory unit stayed in HRS owns a low response to UV light due to the high resistance of memristor at +1 V bias voltage which is below V_{set}. However, the device stayed in LRS exhibits a high response to UV light because both memristor and image sensor remain in a low resistance state. The distinction for photoelectrical response can be used to distinguish whether a light existed to switch resistance states. By periodically switching UV light on/off, the dynamic photocurrent response of the memory unit demonstrates a high stability and good reproducibility under different resistance states. However, an extremely low photoresponse responded to a lower light intensity (e.g., λ = 410 nm, 10.2 μW cm^{-2}) is unable to switch

memristor to LRS resulting from that the high resistance of image sensor leads to a low partial voltage on the memristor which is lower than V_{set} (Figure S13, Supporting Information). The results prove that the photoresponse of image sensor determines the light information stored or not and only the photoresponse reaches to a critical value, memristor can be resistive switching from OFF state to ON state.

For further revealing the stability of reconfigured resistance states, the retention properties are measured under +1 V bias voltage at room temperature (Figure 3d). A long-term retention performance is obtained due to no resistance changes for 1600 s at both HRS and LRS. The switching characteristics reveal the visual memory can achieve the operations of "write" and "erase" under the existence of UV light. During successive 50 voltage sweeping cycles, the HRS and LRS display little vibration within limits and tend to be gradually stabilized (Figure 3e), proving that the bistable memory switching is entirely reversible and reproducible. In addition, V_{set} and V_{reset} during 50 switching cycles are distributed within a range of 1.7 ± 0.4 and -1.6 ± 0.3 V respectively with no tremendous changes occurring (Figure 3f).

The nonvolatile memristor behavior is dominated by the photoelectric response of the series image sensor. At initial state without UV light, both the image sensor and the memristor are located in HRS (Figure 3g). For the memristor, the original resistance is below HRS of the image sensor, thus the partial voltage acquired for memristor cannot reach to V_{set} and induce it from HRS to LRS. When UV light applied, the resistance of the image sensor decreased by the excitation of photon, thus the partial positive voltage of memristor will increase to V_{set} gradually with the increasing of photoresponse. During this process, a positive voltage is applied on Ni top electrode of the memristor, Ni^+ is formed due to the oxidation of Ni electrode. Under the electrical field formed in the memory layer, Ni^+ migrates from the top electrode and will be reduced back to Ni atom after a short-haul movement.[20,34] With the increase of reductive Ni atoms, Ni filaments are finally formed from Ni top to Au bottom electrodes, thus inducing memristor switching from HRS to LRS. At this moment, the current flows through the conductive filament in the solid memory layer and LRS of memristor will maintain for a long time even though removing the UV light or applied voltage. To reprogram the memory device unit, a negative voltage (V_{reset}) is required to erase it from LRS to HRS. During the negative-reset process, the Ni conductive filament nearby Au bottom electrode will be disintegrated in part and migrate back to the direction of top electrode by thermal-assistant electrochemical reaction, thus trigger memristor to HRS.[35,36] Using such method, the visual memory unit can achieve the operations of "write" and "erase" under the existence of UV light. Based on the analysis above, we conclude that the competition of conductive metal nanofilament formation and dissolution exists in the solid memory layer is an intrinsic decisive factor to switch the memory device between HRS and LRS. Meanwhile, the external factor to switch the memory on/off is dominated by the UV light photoresponse of image sensor via achieving sufficient partial voltage in the set/reset process. The large memory window (I_{set}/I_{reset}) between different resistance states at 1 V is above 10^2 during the voltage sweep cycle.

The visual memory device is also fabricated on flexible polyimide substrate to expand the future applications in wearable electronic devices and human bionic devices (Figures S14 and S15, Supporting Information). The results indicate that flexible visual memory device can also work normally with a similar set/reset process and good retention behavior with little fluctuation. Resistance stability in HRS and LRS of flexible memory device as a function of bending angles has been demonstrated from the flat state to 150° bending. These results demonstrate excellent resistive switching characteristic such as long-term retention, good stability, and reproducibility toward UV light, thus providing a practicable way to record the applied UV light by switching resistance states of flexible visual memory unit, which can realize the sensing and memory of UV light information even after removing the exposed UV light. Considering the cost-effective and scalable technology to print aligned SMWs arrays on discretionary substrates, it can guide an effective path for future flexible and wearable devices.

To demonstrate the capability of imaging and memorizing the distribution of external patterned light, flexible visual memory arrays consisting of 10×10 pixels are then fabricated to record the information of applied patterned light. Each pixel is composed of memristor and image sensor to form a circuit in series as a visual memory unit. As illustrated in **Figure 4**a, a diffraction optical element (DOE) with a butterfly pattern inside is utilized to generate a butterfly-like patterned light while a bundle of UV laser entered in the DOE. The butterfly-like patterned light is irradiated on top of the visual memory arrays and the corresponding device unit can sense and record the UV light (Figures S16 and S17, Supporting Information), thus all activated pixels stayed in ON state can constitute the distribution of applied patterned light and the light information can be memorized in the visual memory arrays finally. Figure 4b shows the direct-printing process to fabricate the aligned In_2O_3 SMWs arrays on the memory device by just one time, which reveals the ability of near-field direct-printing system to print large-scale aligned SWMs in desired positions and orientations directly on rigid or flexible substrates. Figure 4c,d shows the digital photos of visual memory arrays with 10×10 pixels fabricated on silica substrate and flexible polyimide substrate.

Figure 4e displays a photograph of the butterfly-shaped pattern generated from irradiating incident UV laser through the patterned DOE. After irradiated on the position of flexible visual memory device in Figure 4a, only those devices exposed under the patterned light show photoresponse to light and can be triggered from HRS to LRS by a positive voltage sweep from 0 to V_{set}. After removing the light, each programmed device unit as one pixel is recorded in the memory arrays and formed the image map by the software "MATLAB" as illustrated in Figure 4e. A legible butterfly-shaped pattern can be observed from the mapping which read from the visual memory arrays, demonstrating the feasible capability of imaging and memorizing when subjected to external stimulation of patterned light. Keeping the device at room temperature for 1 week, the visual memory arrays can still retain the butterfly-shaped pattern from the mapping with little attenuation. To investigate the reversibility and reproducibility of the device arrays, a negative-reset voltage sweep is applied to erase the patterned light information stored in the memory device by switching resistance state from

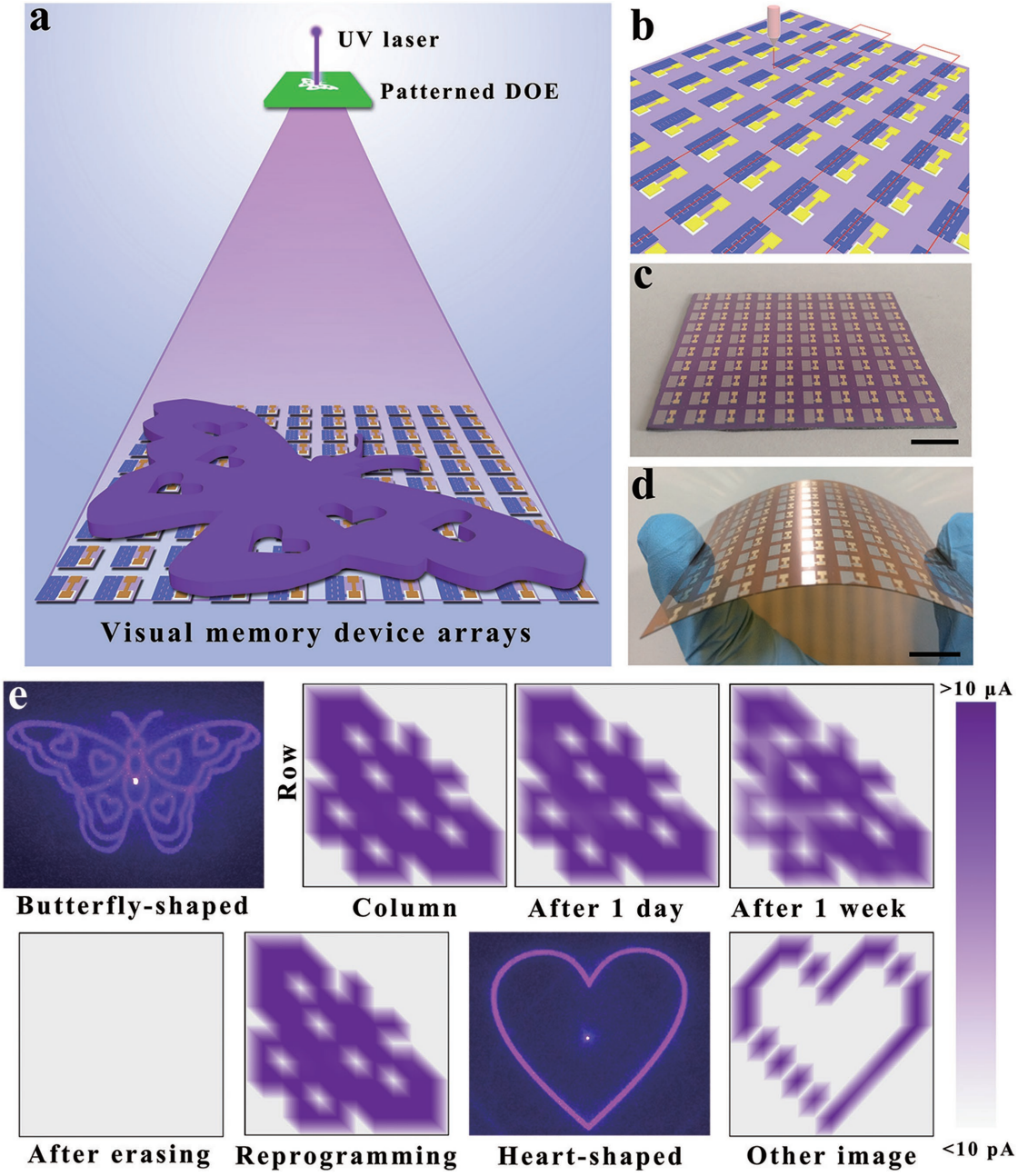

Figure 4. Imaging and memorizing behaviors of the flexible visual memory arrays. a) Schematic diagram to detect and memorize the information of light distribution which generated from a patterned DOE. b) The near-field direct-printing process to prepare In_2O_3 SMWs on visual memory arrays. c,d) Digital photos of the integrated devices arrays on rigid SiO_2 and flexible polyimide substrates, respectively. Scale bar, 1 cm. e) Information storage behaviors and effective reusability of the flexible visual memory device arrays for the applied patterned light. The mappings have executed the interpolation command of "shading interp" to smooth the color transition by MATLAB.

LRS to HRS. After applying the butterfly-like patterned light on the device arrays again at the same position or a heart-shaped light pattern, the imaging information can be easily detected and memorized once more, revealing the capability of write and erase information for multicycle usage. Though the flexible visual memory device with present resolution here can realize the sensing and memory functions for patterned UV light, a higher pixel is indispensable to distinguish more sophisticated light. The results provide a novel idea to mimic human visual memory and promoting flexible integrated memory device in the applications of future wearable devices, bionic device, electronic eyes, and multifunctional robotics, etc.

In conclusion, a facile architecture of visual memory arrays is designed to mimic human visual memory by integrating UV image sensor arrays and resistance switching memristors in series. The image sensor based on printed In_2O_3 SMWs owns a high on/off ratio of up to 10^4 under the UV wavelength of 350 nm and the memory device shows a large memory window

of above 10^2, a long-term retention of at least 1600 s and excellent bistable memory behavior after 50 switching cycles. The light distribution with patterned image can be detected and wrote in the visual memory arrays (10×10 pixels) by expanding the pixels densities of device arrays, and the further improvement of spatial resolution can realize the mimicry for human visual memory to capture and memory high-resolution images. The stored information of light distribution shows a long-term retention performance at least 1 week in the visual memory arrays due to the nonvolatile characteristic of resistance switching memristor. In addition, the visual memory arrays can be reprogrammed by a reset-negative voltage and reproduce the image distribution, which demonstrated the effective reusability. The design of architecture and fabrication of device arrays provide a novel approach to integrate functional sensor and memory device for the imitation of human echoic memory and haptic memory, thus creating new opportunities for the flexible visual memory device to apply in future wearable electronics, electronic eyes, multifunctional robotics, and auxiliary equipment for visually handicapped, etc.

Experimental Section

Equipment Setup: A home-built direct-printing system to fabricate aligned SMWs arrays is illustrated in Figure S2A (Supporting Information). The direct-printing system utilized near-field electrospinning technology and 2D (*X*–*Y* axis) moving platform with high-precision guide rails for each axis. This system could print various aligned organic/inorganic micrometer-sized wires on rigid or flexible substrates. In addition, the system consisted of a syringe mounted vertically over the platform, a microinjection pumped to provide pressure for controlling the flow rate of precursor solution, an ultrafine stainless steel nozzle, a grounded flat substrate which could be moved along the linear *X*–*Y* axis, a high voltage DC power supply with output voltage of 0–30 kV.

Preparation of In_2O_3 SMWs Electrospun Solution: 0.5 g $In(NO_3)_3{\cdot}4.5$ H_2O was added in 5 mL deionized water and 8 mL ethanol mixture under 300 rpm magnetic stirring until dissolved completely. Then, 1.5 g polyvinylpyrrolidone (molecular weight of 1,600,000) was added in the above solution with 300 rpm magnetic stirring for 5 h until a homogeneous and transparent solution was obtained. The precursor solution was used to prepare In_2O_3 SMWs through the direct-printing system.

Near-Field Electrospinning and Direct Printing of Aligned In_2O_3 SMWs Arrays: The distance between the stainless steel nozzle and the grounded substrate was set as 0.5–1.4 mm. The solution falling speed was controlled by microinjection pump. In order to obtain aligned SMWs array, a command program was input into the computer system to control the moving speed and trajectory of *X*–*Y* axis. A high DC voltage of +1.35 kV was applied to the stainless steel nozzle to start the near-field electrospinning and deposit SMWs on substrate under the effect of electric field force. Run the command program, the substrate was shifted with the moving of *X*–*Y* axis and aligned SMWs could be obtained. Through setting the interval of *y* axis between the adjacent two lines, the printing density of SMWs could be controlled as expectation (>5 µm). Then, put samples into the rapid thermal processing system at 400 °C for 1.5 h in air.

Visual Memory Device Fabrication: The integrated device was fabricated by multimask photolithography. First, 30 nm Au pattern film as bottom electrode was deposited on the above substrate with annealed SMWs by photolithography and thermal evaporation. Then, 23 nm Al_2O_3 memory layer was deposited on the bottom electrode by photolithography and atomic layer deposition process (200 °C, 0.15 torr, 0.02s trimethylaluminum, 200 cycles). After that, 70 nm Ni as the top electrode of memristor and two electrodes of image sensor were deposited by photolithography technique and thermal evaporation.

Device Characterization and Measurement: The performances of the image sensor and memristor were performed by probe station with a semiconductor characterization system (Keithley 4200-SCS). For the test of photoelectric performance, a power adjustable homogeneous light source system was utilized as the UV illumination source. The incident UV power was measured by an Ophir NOVA power meter. All measurements were performed in air and at room temperature. For the measurement of visual memory arrays, a 405 nm, 20 mW blue-violet laser was used as light source. The various patterned DOEs were offered by Beijing central press union technology CO., LTD. The surface morphology was observed by AFM (Bruker Multimode 8). The crystalline phase of In_2O_3 was examined via powder X-ray diffraction (Rigaku D/Max-2550).

Supporting Information

Supporting Information is available from the Wiley Online Library or from the author.

Acknowledgements

S.C. and Z.L. contributed equally to this work. This work was supported by the National Natural Science Foundation of China (61625404, 51672308, 61574132, and 61504136), Beijing Natural Science Foundation (4162062), and the Key Research Program of Frontier Sciences, CAS (QYZDY-SSW-JWC004).

Conflict of Interest

The authors declare no conflict of interest.

Keywords

flexible electronics, imaging sensors, resistive switching memristors, UV photodetectors, visual memory

Received: September 19, 2017
Revised: October 12, 2017
Published online:

[1] R. Q. Quiroga, L. Reddy, G. Kreiman, C. Koch, I. Fried, *Nature* **2005**, *435*, 1102.
[2] I. G. Sligte, A. R. E. Vandenbroucke, H. S. Scholte, V. A. F. Lamme, *Front. Psychol.* **2010**, *1*, 175.
[3] J. M. Hillis, M. O. Ernst, M. S. Banks, M. S. Landy, *Science* **2002**, *298*, 1627.
[4] B. W. Zhu, H. Wang, Y. Q. Liu, D. P. Qi, Z. Y. Liu, H. Wang, J. C. Yu, M. Sherburne, Z. H. Wang, X. D. Chen, *Adv. Mater.* **2016**, *28*, 1559.
[5] R. Romo, V. D. Lafuente, *Prog. Neurobiol.* **2013**, *103*, 41.
[6] K. J. Reissner, J. L. Shobe, T. J. Carew, *Cell. Mol. Life Sci.* **2006**, *63*, 963.
[7] C. M. Jiang, J. H. Song, *Adv. Mater.* **2015**, *27*, 4454.
[8] J. Kim, J. Kim, S. Jo, J. Kang, J. W. Jo, M. Lee, J. Moon, L. Yang, M. G. Kim, Y. H. Kim, S. K. Park, *Adv. Mater.* **2016**, *28*, 3078.
[9] W. Deng, X. J. Zhang, L. M. Huang, X. Z. Xu, L. Wang, J. C. Wang, Q. X. Shang, S. T. Lee, J. S. Jie, *Adv. Mater.* **2016**, *28*, 2201.

[10] L. L. Gu, M. M. Tavakoli, D. Q. Zhang, Q. P. Zhang, A. Waleed, Y. Q. Xiao, K. H. Tsui, Y. J. Lin, L. Liao, J. N. Wang, Z. Y. Fan, *Adv. Mater.* **2016**, *28*, 9713.
[11] Y. L. Chu, X. H. Wu, J. J. Lu, D. P. Liu, J. Du, G. Q. Zhang, J. Huang, *Adv. Sci.* **2016**, *3*, 1500435.
[12] H. C. Ko, M. P. Stoykovich, J. Song, V. Malyarchuk, W. M. Choi, C.-J. Yu, J. B. Geddes III, J. Xiao, S. Wang, Y. Huang, J. A. Rogers, *Nature* **2008**, *454*, 748.
[13] J. Borghetti, G. S. Snider, P. J. Kuekes, J. J. Yang, D. R. Stewart, R. S. Williams, *Nature* **2010**, *464*, 873.
[14] R. Waser, R. Dittman, G. Staikov, K. Szot, *Adv. Mater.* **2009**, *21*, 2632.
[15] J. J. Yang, M. D. Pickett, X. M. Li, D. A. A. Ohlberg, D. R. Stewart, R. S. Williams, *Nat. Nanotechnol.* **2008**, *3*, 429.
[16] H. S. P. Wong, S. Salahuddin, *Nat. Nanotechnol.* **2015**, *10*, 191.
[17] L. O. Chua, *Appl. Phys. A* **2011**, *102*, 765.
[18] D. Kuzum, R. G. D. Jeyasingh, B. Lee, H. S. P. Wong, *Nano Lett.* **2012**, *12*, 2179.
[19] S. H. Jo, T. Chang, I. Ebong, B. B. Bhadviya, P. Mazumder, W. Lu, *Nano Lett.* **2010**, *10*, 1297.
[20] J. J. Yang, D. B. Strukov, D. R. Stewart, *Nat. Nanotechnol.* **2013**, *8*, 13.
[21] T. Ohno, T. Hasegawa, T. Tsuruoka, K. Terabe, J. K. Gimzewski, M. Aono, *Nat. Mater.* **2011**, *10*, 591.
[22] M. Lorenz, M. S. R. Rao, T. Venkatesan, E. Fortunato, P. Barquinha, R. Ranquinho, D. Salgueiro, R. Martins, E. Carlos, A. Liu, F. K. Shan, M. Grundmann, H. Boschker, J. Mukherjee, M. Priyadarshini, N. DasGupta, D. J. Rogers, F. H. Teherani, E. V. Sandana, P. Bove, K. Rietwyk, A. Zaban, A. Veziridis, A. Weidenkaff, M. Muralidhar, M. Murakami, S. Abel, J. Fompeyrine, J. Z. Perez, R. Ramesh, N. A. Spaldin, S. Ostanin, V. Borisov, I. Mertig, V. Lazenka, G. Srinivasan, W. Prellier, M. Uchida, M. Kawasaki, R. Pentcheva, P. Gegenwart, F. M. Granozio, J. Fontcuberta, N. Pryds, *J. Phys. D: Appl. Phys.* **2016**, *49*, 433001.
[23] L. L. Wang, D. Chen, K. Jiang, G. Z. Shen, *Chem. Soc. Rev.* **2017** https://doi.org/10.1039/c7cs00278e.
[24] X. Liu, L. L. Gu, Q. P. Zhang, J. Y. Wu, Y. Z. Long, Z. Y. Fan, *Nat. Commun.* **2014**, *5*, 4007.
[25] S. Y. Min, T. S. Kim, B. J. Kim, H. Cho, Y. Y. Noh, H. Yang, J. H. Cho, T. W. Lee, *Nat. Commun.* **2013**, *4*, 1773.
[26] S. Y. Kim, K. Kim, Y. H. Hwang, J. Park, J. Jang, Y. Nam, Y. Kang, M. Kim, H. J. Park, Z. Lee, J. Choi, Y. Kim, S. Jeong, B. S. Bae, J. U. Park, *Nanoscale* **2016**, *8*, 17113.
[27] D. H. Reneker, A. L. Yarin, H. Fong, S. Koombhongse, *J. Appl. Phys.* **2000**, *87*, 4531.
[28] A. Lee, H. Jin, H. W. Dang, K. H. Choi, K. H. Ahn, *Langmuir* **2013**, *29*, 13630.
[29] D. Zhang, C. Li, S. Han, X. Liu, T. Tang, W. Jin, C. Zhou, *Appl. Phys. A* **2003**, *76*, 1.
[30] R. A. Ismail, A. K. Ali, K. I. Hassoon, *Opt. Laser Technol.* **2013**, *51*, 1.
[31] D. L. Shao, L. Q. Qin, S. Sawyer, *Appl. Surf. Sci.* **2012**, *261*, 123.
[32] S. Y. Huang, G. Ou, J. Cheng, H. P. Li, W. Pan, *J. Mater. Chem. C* **2013**, *1*, 6463.
[33] R. Martins, P. Barquinha, A. Pimentel, L. Pereira, E. Fortunato, D. Kang, I. Song, C. Kim, J. Park, Y. Park, *Thin Solid Films* **2008**, *516*, 1322.
[34] S. Liu, N. D. Lu, X. L. Zhao, H. Xu, W. Banerjee, H. B. Lv, S. B. Long, Q. J. Li, Q. Liu, M. Liu, *Adv. Mater.* **2016**, *28*, 10623.
[35] Q. Liu, Y. Sun, H. B. Lv, S. B. Long, K. B. Yin, N. Wan, Y. T. Li, L. T. Sun, M. Liu, *Adv. Mater.* **2012**, *24*, 1844.
[36] T. Tsuruoka, I. Valov, S. Tappertzhofen, J. V. D. Hurk, T. Hasegawa, R. Waser, M. Aono, *Adv. Funct. Mater.* **2015**, *25*, 6374.

